Materials Science, Vol. 32, No. 1, 1996

ON THE INTERACTION OF CRACKS WITH BIMATERIAL INTERFACES

R. O. Ritchie

Mechanical properties of engineering materials are primarily controlled by interfaces that they contain, i.e., free surfaces, grain boundaries, and phase boundaries. The fracture and fatigue properties, in particular, are a function of the interaction of such boundaries with cracks. In the present paper, we review the various types of interaction between cracks propagating at or near such bimaterial interfaces. Indeed, the nature of these interactions is critical in determining trajectories of cracks in both homogeneous and layered structures, which in turn has a direct influence on their fracture toughness and resistance to subcritical crack growth.

Introduction

The mechanical integrity and lifetime of most engineering materials, wear/thermal protective coatings, and microelectronic components invariably depend on the nature of interfaces that they contain. In particular, the strength and crack-propagation behavior of metal- and intermetallic-matrix composites and laminates are not generally limited by bulk properties but rather by the *local* interaction of cracks with such interfaces. This in turn is controlled by such factors as the relative strength of the interface and the matrix and reinforcement phases, and the elastic compliance and thermal-expansion mismatch across the interface, which generally dictates the nature of the crack path.

The selection of a crack trajectory in such bimaterial layered or sandwich structures is determined by a mutual competition between the direction of "maximum" mechanical driving force and the "weakest" microstructural path [1]. If the directional and microstructural resistance effects are commensurate, stable crack extension, often at low energy, ensues; where the two effects are incommensurate, erratic, often unstable, crack extension, generally with far higher fracture energies, is obtained [1, 2]. Various criteria have been hypothesized to define the driving force directionality. For entirely linearly elastic homogeneous materials, these proposals include that cracks follow a path of maximum tangential stress, or, equivalently, zero shear stress [3], or proceed along a direction of the maximum mode I stress intensity, KI, vanishing shear stress intensity (i.e., $K_{II} = 0$), or maximum strain-energy release rate G_{max} [4–7]. All these criteria have been shown to be essentially identical for slightly curved cracks under in-plane loading. However, for large shear loadings and resultant large kink angles, the planes given by the latter conditions are still practically (but not exactly) identical [5–11], but define a larger kink angle than do the radial planes given by the first mentioned stress-based criteria [3]. In addition, for larger kinks, the optimal angle changes significantly [5–10] in a manner which can be anticipated from the effect of the T stress (the second nonsingular term in the Williams expansion), which depends upon the specimen geometry and parallel residual stresses [5, 12, 13]. Similarly, for semibrittle materials in which the critical kinking angle is supposed to be dictated by the tangential stress at a critical distance ahead of the crack tip, nonsingular stresses cause measurable differences in kinking angle [14–16].

For interface cracks, similar criteria for kinking off the interface have been evaluated [11], but application is far more complex owing to the spatial variability of stress fields inherent to interface cracks [17]. Combining asymptotic solutions for cracks near interfaces [18] with asymptotic solutions for interface cracks [13] can provide insights as to the expected trends in behavior with respect to the directionality of driving force [1, 2].

Material Sciences Division, Lawrence Berkeley National Laboratory, and Department of Material Science and Mineral Engineering, University of California, Berkeley, CA 94720, USA. Published in Fizyko-Khimichna Mekhanika Materialiv, Vol. 32, No. 1, pp. 119–132, January–February, 1996. Original article submitted October 2, 1995.

1068-820X/96/3201-0107 $15.00

Crack-Tip Fields

The elastic compliance discontinuity across a bimaterial interface modifies the stress field for cracks located at or near the interface. Crack-tip fields for such interfacial and near-interfacial cracks, which have been expressed by using linear elastic and nonlinear elastic fracture mechanics [3–6, 9], show that the ratio of normal to shear stresses ahead of the tip can vary markedly from that induced solely by the (applied) far-field loading. For the determination of crack trajectories, the characterization of these local fields is vital as the local stresses dictate the preferred direction for crack extension.

Interface Cracks. For a crack on the interface between two isotropic homogeneous elastic solids (Fig. 1a), the near-tip stress intensity, which describes important aspects of the near-tip stress field, is conveniently expressed in complex notation as $K = K_1 + iK_2$, where $i = \sqrt{-1}$. The effect of the difference in elastic properties across the interface on the crack-tip fields, termed the elastic modulus mismatch effect, may be described by using two dimensionless Dundurs' parameters, α and β, which are defined as follows [20]:

$$\alpha = \frac{E_1' - E_2'}{E_1' + E_2'}, \tag{1}$$

$$\beta = \frac{1}{2}\frac{\mu_1(1-2\nu_2) - \mu_2(1-2\nu_1)}{\mu_1(1-\nu_2) + \mu_2(1-\nu_1)}, \tag{2}$$

where E_i' are Young's moduli E in plane stress and $E/(1-\nu^2)$ in plane strain, μ_i and ν_i are, respectively, the shear moduli and Poisson's ratios, and the subscripts $i = 1, 2$ refer to materials above and below the crack. By using this definition of α and β, the stress intensity for a crack on the interface, K_1 and K_2, may be expressed in terms of the far-field modes I and II stress intensities, K_I^∞ and K_{II}^∞, as [13]

$$K_1 + iK_2 = g(\alpha, \beta)(K_I^\infty + iK_{II}^\infty)L^{-i\varepsilon}e^{i\omega(\alpha,\beta,L)}, \tag{3}$$

where

$$\varepsilon = \frac{1}{2\pi}\ln\left(\frac{1-\beta}{1+\beta}\right)$$

and $g(\alpha, \beta)$ is a geometry-specific function of the elastic mismatch. The function $\omega(\alpha, \beta, L)$ may be thought of as a *phase shift,* which describes the rotation of the stress field, at a specified distance L from the crack tip, relative to that expected from the far-field loading. This orientation of the stress field is reflected in the ratio of shear to normal stresses acting on the interface which may depend upon the specified distance x ahead of the crack tip [13]; commonly, this ratio is expressed as a *phase angle,* ψ:

$$\psi = \tan^{-1}\left(\frac{\sigma_{xy}}{\sigma_{yy}}\right)_x = \tan^{-1}\left(\frac{\mathrm{Im}(Kx^{i\varepsilon})}{\mathrm{Re}(Kx^{i\varepsilon})}\right), \tag{4a}$$

and, equivalently, from (3)

$$\psi = \tan^{-1}\left(\frac{K_{II}^\infty}{K_I^\infty}\right) + \omega(\alpha, \beta, L) + \varepsilon\ln\left(\frac{x}{L}\right). \tag{4b}$$

It can be seen that the spatial variability in near-tip normal and shear stresses depends only on β through the oscillation index ε. Thus, as conventionally defined [13, 18], the crack-tip stress intensities K_1 and K_2 are strictly determinate only if $\beta = 0$, whereas the interfacial stresses are uniquely determined in terms of the geometry and far-field loading.

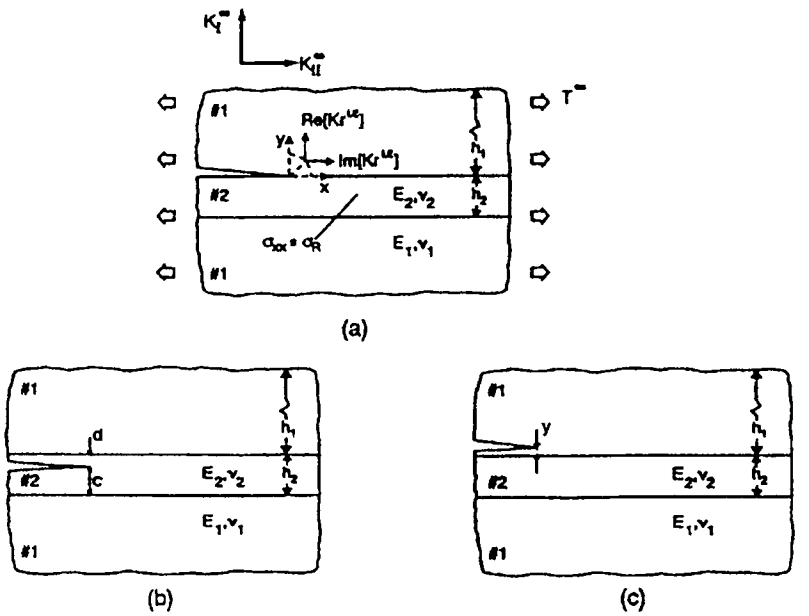

Fig. 1. Conventions for crack tip (a) at the interface between two linear-elastic materials 1 and 2 with Young's moduli E_i and Poisson's ratios ν_i, (b) nearly parallel and close to the interface in the layer of material 2 sandwiched between material 1, and (c) nearly parallel and close to the interface outside the layer of material 2.

Near-Interface Cracks. For a bimaterial sandwich geometry (Fig. 1) of the system consisting of two linear-elastic materials subjected to remote loading defined by the far-field stress intensities, K_I^∞ and K_{II}^∞, the local crack-tip stress intensities K_I and K_{II} for a crack nominally parallel to, and just above, the top interface (Fig. 1c) may be expressed as [1]

$$K_I + iK_{II} = (K_I^\infty + iK_{II}^\infty)\left(\frac{Y}{h_2}\right)^{i\varepsilon} e^{i(\omega_h - \varphi_-)}, \tag{5}$$

and the phase angle of the loading at the crack tip becomes

$$\psi = \tan^{-1}\left(\frac{K_{II}^\infty}{K_I^\infty}\right) - \varphi_- + \omega_h + \varepsilon \ln\left(\frac{Y}{h_2}\right), \tag{6}$$

provided the layer thickness h_2 and the distance from the layer to the crack Y are small compared to all other in-plane dimensions, and $Y/h_2 << 1$. Equation (5) was obtained by using the relationship between the crack-tip stress intensities for a crack just below the interface and those for a similarly loaded crack exactly on the interface from Hutchinson, Mear, and Rice [18]. This relationship has an adjustment in magnitude and phase shift, including the normalizing function $\varphi(\alpha, \beta)$ which is tabulated in [18]. Here, $\varphi_- = \varphi(-\alpha, -\beta)$. Equation (5) also incorporates the explicit solution for a crack on the top interface of a thin sandwiched layer from [21], wherein the shift function $\omega_h(\alpha, \beta)$ for $L = h_2$ is tabulated.

The corresponding solution for the crack within the layer, again nominally parallel and close to the interface, i.e., where h_2/a and $c/h_2 << 1$ in Fig. 1b [13, 18], has the form

$$K_I + iK_{II} = \left[\frac{1-\alpha}{1+\alpha}\right]^{1/2} (K_I^\infty + iK_{II}^\infty)\left(\frac{c}{h_2}\right)^{-i\varepsilon} e^{-i(\varphi_h + \omega)}, \tag{7}$$

where ψ is given by

$$\psi = \varepsilon \ln\left(\frac{h_2 - c}{c}\right) + 2\left[\left(\frac{c}{h_2}\right) - \frac{1}{2}\right][\varphi_h(\alpha, \beta) + \omega(\alpha, \beta)], \tag{8}$$

and the functions $\varphi_h(\alpha, \beta)$ and $\omega(\alpha, \beta)$ are tabulated [18, 21].

Nonlinear Elastic Fields and Crack-Tip Plasticity. Solutions for interface cracks where one material plastically deforms have been derived by Shih and co-workers [22, 23]. However, if small-scale yielding prevails, i.e., the plastic zone is much less than the characteristic dimension, $r_p << L$, then the stress distributions are approximately determined by the linear elastic solutions given above.

For an interface crack loaded in tension between a rigid substrate and an elastic–plastic solid obeying the Ramberg–Osgood constitutive law $\sigma/\sigma_0 = e/e_0 + k(\sigma/\sigma_0)^n$, where k is the order unity and $e_0 = \sigma_0/E$, the small-displacement-gradient near-tip field is of the HRR type [22, 23]:

$$\sigma_{ij} = \sigma_0\left(\frac{J}{k\sigma_0 e_0 r}\right)^{1/(n+1)} f_{ij}(\theta, r, \xi, n), \tag{9}$$

J is Rice's J-integral, $\xi = \psi + \varepsilon \ln[|K|^2/(\sigma_0^2 L)]$ is a dimensionless number representing the traction ratio $\tan^{-1}(\sigma_{xy}/\sigma_{yy})$ at the distance $r = (|K|/\sigma_0)^2$, just outside the plastic zone, σ_0 is the lower yield strength of either material, and f_{ij} is a bounded function dependent upon the plastic mode mixity.

Solutions for interface cracks in the presence of finite-deformation effects, i.e., within the plastic zone, are bounded by the length scales, r_p and δ_t, where δ_t is the crack-tip opening displacement. Solutions for the plastic-zone size give

$$r_p = \chi_1\left(\frac{|K|}{\sigma_0}\right)^2, \tag{10}$$

where the dimensionless factor χ_1, which depends upon mode mixity and, to a lesser extent, on material constants, varies from -0.15 to -0.65 as $|\xi|$ increases from 0 to $\pi/2$ [24]. The crack-tip opening displacement, conversely, is given by

$$\delta_t = \chi_2\left(\frac{J}{\sigma_0}\right), \tag{11}$$

where χ_2 varies from 0.5 to 0.7 for $|\xi| \leq \pi/6$ (for a strain hardening exponent, $n \leq 0.1$). The values of the length scales, r_p and δ_t, differ by a factor comparable with σ_0/E [24].

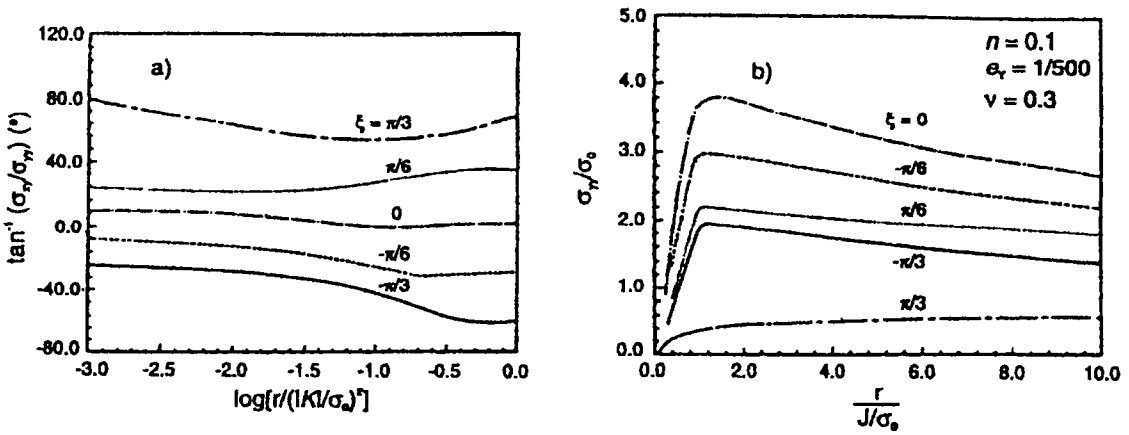

Fig. 2. (a) Ratio of shear stress to tension stress, σ_{xy}/σ_{yy}, and (b) the normalized tensile (hoop) stress, σ_{yy}/σ_0, ahead of a crack tip on the metal/ceramic interface, in the range $\delta_t \le r \le r_p$. Metal properties are $n = 0.1$, $\sigma_0/E = 0.002$, and $\nu = 0.3$ (after [24]).

Solutions are shown in Fig. 2, where the traction ratio, σ_{xy}/σ_{yy}, and normalized tensile (hoop) stress, σ_{yy}/σ_0, are plotted ahead of the blunted crack tip on the interface within $\delta_t < r < r_p$. For far-field mode I loading where $\xi = 0$, the traction ratio remains close to zero; under mixed-mode loading, however, a moderate variation is seen (Fig. 2a). For the tensile stress distribution (Fig. 2b), the maximum hoop stress is reached at $r \approx J/\sigma_y$. At distances closer to the tip, the blunted crack acts to relieve a constraint resulting in lower tensile stresses. It should be noted that the stiffer substrate provides additional constraint to the plastic zone which raises the stress some 10 % compared to that in a homogeneous material (at $\xi = 0$); where higher applied shear stresses are present, this constraint is partially relieved. Under cyclic loading, crack-tip fields ahead of a nonmoving interface crack are essentially identical to that shown in Fig. 2a (for $\xi = 0$) over a major portion of the plastic zone during the initial loading cycle; however, on unloading, a mixed-mode field is generated, inducing strong shear tractions ahead of the crack tip [25].

Crack Trajectories

The trajectory of a crack in a homogeneous material or a dissimilar material layered structure is controlled by the mutual competition of two primary factors: the direction in which the fracture-mechanics driving force is highest and the direction where the microstructural resistance is lowest. As noted above, for linearly elastic homogeneous materials, these criteria include cracking along paths of

– maximum tangential stress or, equivalently, zero shear stress [3],

– maximum mode I stress intensity, K_I,

– zero mode II stress intensity, $K_{II} = 0$, or

– maximum strain-energy release rate, G_{max} [4–7].

These criteria are essentially identical for slightly curved cracks under in-plane loads. For example, for a crack kinking through an angle Ω from its plane (Fig. 3a), the local stress intensities at the crack tip, K_1 and K_2, can be computed from the far-field K_I^∞ and K_{II}^∞ values [7] and used to calculate $G = (K_1^2 + K_2^2)/E'$ (provided the kink size is small compared to all in-plane lengths). The resulting kink angles, computed for $K_{II} = 0$ and at maximum G_{max}, are nearly coincident; in fact, only at phase angles greater than $\sim 50°$, the difference is greater than one degree (Fig. 3b) [26]. Thus, for all practical purposes, there is no distinction between the criteria listed above.

Cracks Near Interfaces. Cracks Impinging Interfaces. A crack which impinges on an interface between two dissimilar elastic materials may

– arrest,

– penetrate the interface, or

– deflect into the interface.

Whether the crack penetrates or deflects along the interface between two isotropic elastic solids is again both a function of relative microstructural resistance and magnitude of the relevant crack-driving forces. This competition has been analyzed [27] by comparing the energy release rate for the interfacially deflected crack, G_{IF}, with the maximum energy release rate for a penetrating crack, G_{max}, in order to derive the range of toughnesses of the interface relative to that of the bulk material for each mode of behavior.

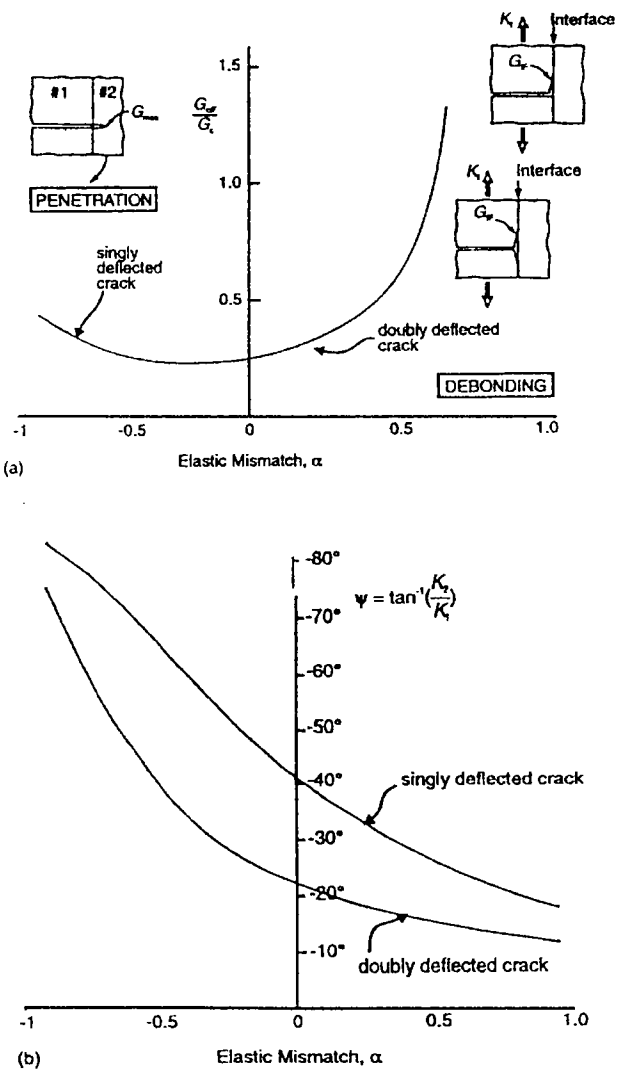

Fig. 5. (a) Crack front debond v. penetration diagram indicating relative interfacial fracture energies, G_{eff}/G_c, in which debonding occurs in preference to penetration of the interface; (b) trends in phase angle ψ with the debonded crack with elastic mismatch α [27].

For the configuration of a crack approaching the interface from material #1 to #2, the impinging crack will likely be deflected along the interface if G_{IF}/G_{max} exceeds the ratio of the interface to matrix (material #2) fracture toughnesses, G_{cIF}/G_c, at the relevant phase angle ψ, i.e., that Eq. (12) applies; conversely, the crack will penetrate the interface when the equality is reversed [27]. Solutions to this problem (with $\beta = 0$) for a crack subjected to mode I loading are given in Fig. 5. For the crack initially aligned perpendicular to the interface (with $\alpha \sim 0$), Fig. 5a indicates that, provided the fracture toughness of the interface is less than one fourth of the matrix toughness of material #2, the crack will deflect at the interface, i.e., when $G_{cIF}/G_c < 1/4$ (note that G_{cIF} depends strongly on ψ). The critical ratio increases to $\sim 1/2$ when $\alpha = 1/2$, corresponding to a plane strain Young's modulus of material #1 being three times that of material #2.

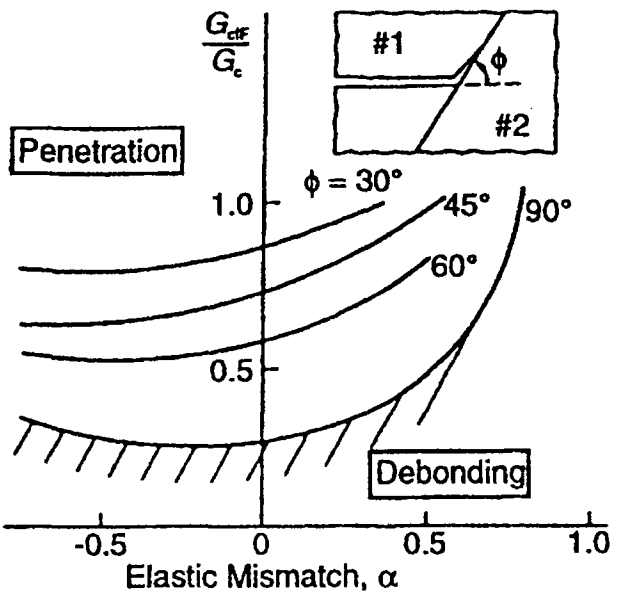

Fig. 6. Effect of the orientation of the crack relative to the interface on the requirements for debonding versus penetration [27, 28].

For a crack approaching the interface obliquely, G_{IF}/G_{max} increases as the interface angle φ decreases (Fig. 6). Consequently, deflection along the interface occurs at higher values of G_{cIF}/G_c [27, 28].

These criteria are critically important in the understanding of the fracture and fatigue properties of fiber-reinforced composites and laminates where delamination at the fiber/matrix interface, as opposed to failure of the fiber, can result in significantly improved crack-growth resistance [28].

Crack Nearly Parallel to an Interface. Considering first the nature and stability of the crack path in layered or sandwich structures where the crack exists close, and nearly parallel, to an interface [1, 2, 29], such as that depicted in Fig. 1b, under pure mode I far-field loading ($K_{II}^{\infty} = 0$), linear-elastic analysis would dictate that a straight crack *within* the central layer #2 would sit along the centerline ($c/h_2 = 0.5$) to satisfy the $K_{II} = 0$ condition. Note that to preserve stability a compressive T-stress must also exist, as the presence of a positive T-stress results in a tendency for this crack path to become unstable [7]. For a crack above the centerline, kinking down toward the centerline will occur if $K_{II} > 0$. In general terms (Fig. 1c), the $K_{II} = 0$ criterion implies that straight cracks misplaced from the centerline (i.e., the $K_{II} = 0$ path) will only head toward the centerline if the K_{II}-derivative is positive, i.e., $\partial K_{II}/\partial c > 0$. If $\partial K_{II}/\partial c < 0$, the negative K_{II} will drive the crack away from this preferred path and the crack will kink toward the interface. However, as shown below, with certain layered material combinations, an additional straight crack path satisfying the $K_{II} = 0$ criterion is found away from the centerline close to one of the interfaces.

In general, for a given bimaterial couple with a strong interface, subjected to applied (far-field) mode I or mixed-mode loading, the expected trends in crack paths can be deduced from the sign of K_{II}, the location of the preferred $K_{II} = 0$ paths for straight parallel cracks, and the sign of the K_{II}-derivative, $\partial K_{II}/\partial c$. The sign of the K_{II} derivative is an important consideration for determining the trajectories of cracks initially misplaced or perturbed from a $K_{II} = 0$ path; such cracks are only able to reach the $K_{II} = 0$ path if this gradient is positive [29]. These factors can be determined from the relevant crack-tip field solutions for near-interface cracks [18] and sandwich layers, e.g., Eq. (7) for cracks within the central layer #2 (Fig. 1b), and Eq. (5) for cracks outside this layer (Fig. 1c), and depend solely upon the elastic mismatch (Dundurs') parameters α and β. Thus, by using this approach and assuming that linear-elastic conditions prevail, it is possible to predict the likely crack path for all bimaterial combinations in terms of their relative elastic moduli and Poisson's ratios.

Thus, we can generate crack-path predictions based on asymptotic straight crack analyses for cracks initially inside and outside the metal layer #2 in a ceramic/metal sandwich geometry for all possible combinations of the modulus mismatch parameters. Derived below are plane-strain solutions where the far-field loading is pure mode I.

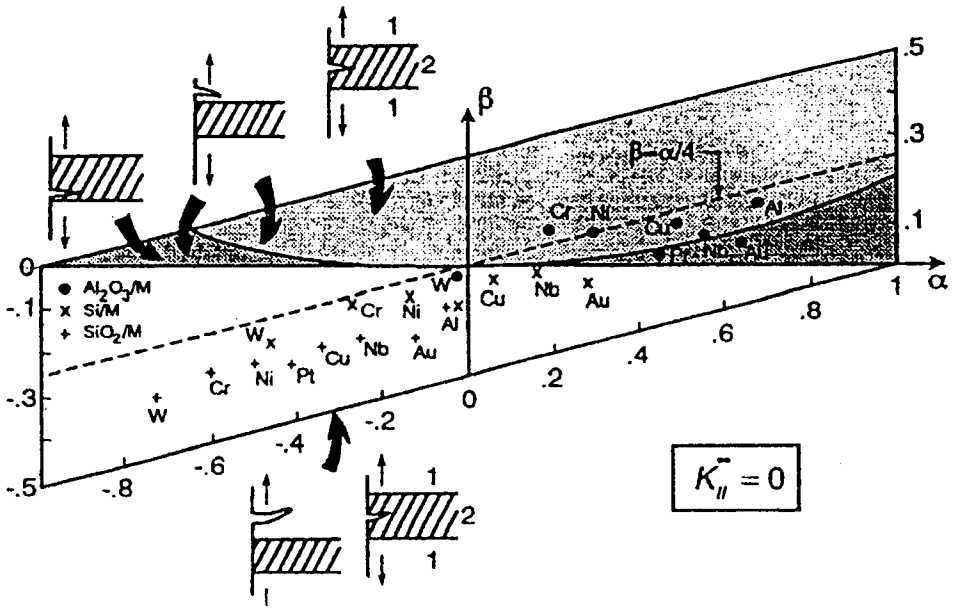

Fig. 7. Plot of the elastic mismatch (Dundurs') parameters α and β in plane strain, showing three predicted regimes of crack-path trajectories with $K_{II} = 0$ for ceramic/metal sandwich geometries subjected to far-field mode I loading [1, 2].

Cracks within the Metal Layer. For cracks initiated within the metal layer (Fig. 1b), the location c/h_2 of the path where $K_{II} = 0$, and the nature of the K_{II}-derivatives can be derived from Eqs. (7) and (8) in terms of all possible combinations of α and β. Three general regimes of expected behavior are found; these are plotted in the α/β space in Fig. 7 [1, 2, 29]. For $\beta < 0$ with any value of α (e.g., metal bonded to silica), as shown by the lighter hatched region in Fig. 7, the centerline of the metal layer satisfies $K_{II} = 0$ but is an unstable path in the sense that $\partial K_{II}/\partial c < 0$. Accordingly, the driving force for cracks preexisting within the metal layer will tend to deflect these cracks toward the interface, whereas near-interface cracks in ceramic substrates will have a tendency to deflect away from the interface. This behavior should be shown by geometries consisting of metal layers sandwiched between more compliant glass substrates (e.g., a Cu layer sandwiched between glass or silicon substrates).

For $\beta > 0$ (e.g., metal bonded to alumina), the centerline of the metal layer again satisfies $K_{II} = 0$, but the gradient $\partial K_{II}/\partial c$ in this vicinity is only positive for the range of values of α shown by the darker hatched area in Fig. 7. In this regime, the crack should seek the center of the metal layer. If it lies off the center within the metal layer, it should kink toward the centerline because of the positive K_{II}, whereas if it preexists outside the layer in the

substrate, it should be drawn into the interface. Examples of this behavior should be seen with metal layers sandwiched between stiffer ceramic substrates, such as Al_2O_3–Cu and Al_2O_3–Al.

For the remaining values of α with $\beta > 0$, shown by the two unhatched regions in Fig. 7, three locations within the layer satisfy $K_{II} = 0$, namely, the centerline at $c/h_2 = 0.5$ (but this represents an unstable path in the sense that $\partial K_{II}/\partial c < 0$) and two other locations close to the interface where $c/h_2 \to 0$ or 1, both of which are stable as $\partial K_{II}/\partial c > 0$. In this regime, which should be seen in Al_2O_3–Au and Al_2O_3–Pt, cracks should follow a trajectory in the metal parallel but close to the interface.

Cracks outside the Metal Layer. For cracks initially outside the metal layer (Fig. 1c), similar predictions, now based on Eqs. (5) and (6), suggest that only two regimes of behavior exist (Fig. 7) [1, 2]. For $\beta > 0$, a positive gradient in K_{II} exists for cracks initiated above the layer such that they should be drawn to the interface with the metal layer. Conversely, for $\beta < 0$, a negative K_{II} suggests that cracks should deflect away from the interface into the ceramic.

Comparison with Experiment

"Weak" Interfaces. The presence of a "weak" interface generally results in interfacial failure. Such a behavior is invariably shown by glass/Cu bonds, where $\beta < 0$, and depending on the processing, on occasion by Al_2O_3/Cu, Al_2O_3/Au, and Al_2O_3/Pt bonds, where $\beta > 0$ [1, 2]. However, with somewhat better bonding, particularly with a tougher metal, or following interactions with defects in the vicinity of the interface, the interfacial cracks in these systems often deflect into the ceramic, with their subsequent behavior depending upon the sign of β.

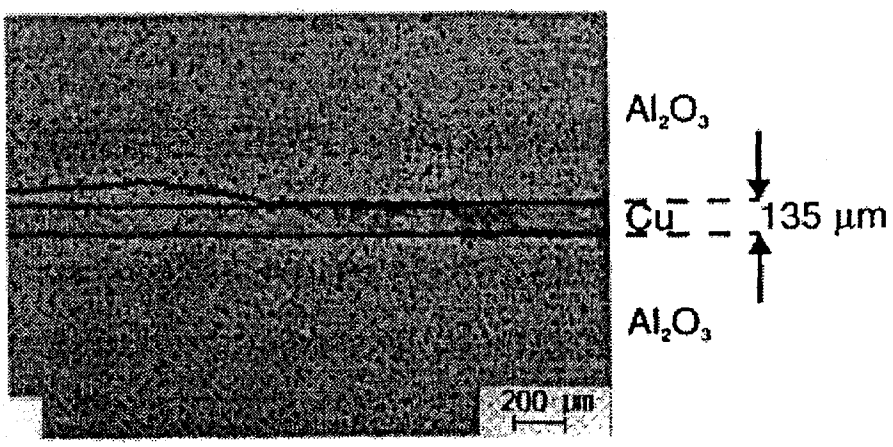

Fig. 8. Scanning electron image of crack path in Al_2O_3/Cu/Al_2O_3 ($\beta > 0$) $C(T)$ sandwich sample, showing predominantly interfacial failure with deflected cracks being drawn back to the interface. This cracking morphology effectively "plucks" pieces out of the ceramic [2].

Where cracks are deflected from the interface into the ceramic, it would be anticipated from consideration of the $K_{II} = 0$ path and the signs of K_{II} and $\partial K_{II}/\partial c$ (Fig. 7) that in the glass/Cu system, the crack should kink away from the interface as $\beta < 0$, which in fact is what is seen [1, 2, 30]. Conversely, with the Al_2O_3/metal systems where $\beta > 0$, cracks deviated from the interface are drawn back again, so that pieces of the ceramic are plucked out, as illustrated for Al_2O_3/Cu interfaces in Fig. 8.

A further demonstration of the prominent role of β in dictating whether cracks are drawn to, or deflected away from, the ceramic/metal interface is shown by results from the 4-point bend tests on glass-Cu ($\beta < 0$) and Al_2O_3/Al ($\beta > 0$) sandwich specimens, where notches placed in the ceramic substrate initiated cracking at varying

distances from the interface. Results [30] shown in Fig. 9 clearly indicate that in Al_2O_3/Al samples, the effect of the positive β is the draw cracks in the ceramic into the interface (Fig. 9a); in fact, cracks which initiate at distances of over four times the metal-layer thickness are attracted to the metal layer. Conversely, where β is negative in glass/Cu/glass specimens, cracks initiated in the glass at the interface and up to three times the metal-layer thickness away are all deflected away from the metal layer (Fig. 9b). Numerical computations for both the Al_2O_3/Al and glass/Cu systems show that the local phase angle, $\psi = \tan^{-1}(K_{II}/K_I)$, for these crack trajectories is within $-1°$ near zero, indicating that the cracks do indeed follow a path dictated by the $K_{II} = 0$ criterion [30].

Clearly, with "weak" interface systems, the crack trajectory is generally along the interface because the microstructural crack-path resistance is lower there; cracks in the ceramic will only find the interface if the compliance mismatch is such that $\beta > 0$.

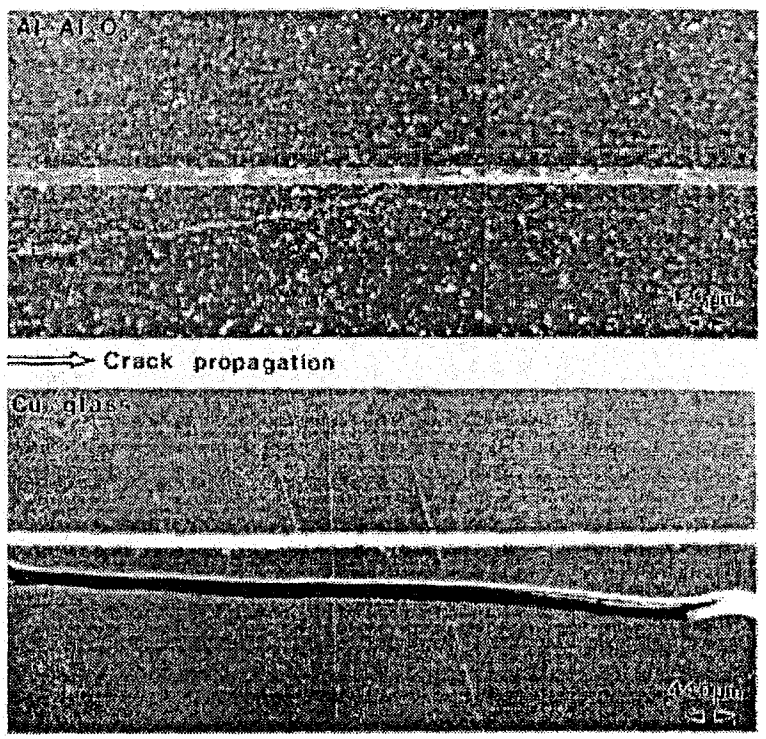

Fig. 9. Scanning electron micrographs of the crack-path profiles showing cracks (a) being drawn to the metal layer with Al_2O_3/Al ($\beta > 0$), and (b) deflected away from the layer in glass/Cu ($\beta < 0$) [30].

"Weak" Metal. An example where cracking in ceramic/metal/ceramic layered structures is confided to the metal layer is shown by the $\beta < 0$ system Al_2O_3/Al. For such a configuration, Fig. 7 predicts a stable $K_{II} = 0$ path down the center if $\beta/|\alpha|$ exceeds a critical range versus stable $K_{II} = 0$ paths near either interface if $\beta/|\alpha|$ is less, but positive, i.e., the darker hatched region versus the unhatched region in Fig. 7. Therefore, on the basis of α and β values of $+0.686$ and $+0.143$, respectively, for the Al_2O_3/Al system, a centered crack within the metal layer is predicted. Contrary to these predictions, however, cracks in Al_2O_3/Al flexure samples generally propagate in the pure aluminum but well off the centerline within $\sim 50\,\mu m$ or so of the interface (Fig. 10) [1, 2]. Whereas this effect could be associated with easier initiation in the vicinity of the interface, the prime cause may be associated with the inevitable presence of plasticity in metal. Since crack-tip plasticity would have the effect of making the metal more compliant and incompressible, the observed cracking configurations would be anticipated simply by decreasing E_{Al} and increasing $\nu_{Al} \to 0.5$. Crack paths near the interface would then be predicted since $\alpha \to 1$ and $\beta \to 0$; $2E_{Al}/3$ and the self-consistent $\nu_{Al} \sim 0.4$ are sufficient.

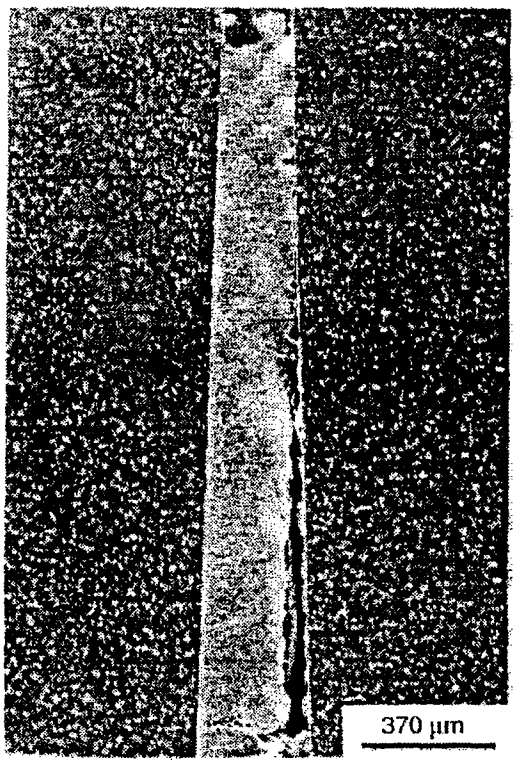

Fig. 10. Scanning electron image of an Al_2O_3/pure Al/Al_2O_3 ($\beta > 0$) 4-point bend sandwich sample, showing failure in the pure aluminum. Note that cracking in the metal layer proceeds near the interface and not along the centerline [1].

"Weak" Ceramic. Where the ceramic provides a weaker microstructural crack path, cracking predominates in this phase and the crack path generally conforms to the linear-elastic predictions of Fig. 7. For example, as described above, the modulus mismatch acts to drive cracks away from the metal layer into the ceramic where $\beta < 0$, i.e., in glass/Cu sandwich samples (Fig. 9b), resulting in a low toughness of the joint. Where $\beta > 0$, cracks are conversely attracted to the metal layer and tend to pluck out pieces of the ceramic, as shown by the Al_2O_3/Cu system in Fig. 8. In fact, in the positive β system, cracks are drawn away from the weaker microstructural path in the ceramic to the stronger interface and metal, and can often blunt out in the metal phase with resulting high toughness. In these cases, the mutually opposing influence on the crack path of the lowest microstructural resistance and highest crack-tip driving force (due to far-field loading and modulus mismatch effects) generally results in complex cracking configurations with high yet erratic toughness values [1, 2].

SUMMARY

1. Asymptotic crack-tip field solutions are available for cracks at, or near, bimaterial interfaces separating linear elastic, and to a limited extent, elastic/plastic materials. The compliance discontinuity across the interface modifies the stress fields, such that the ratio of normal to shear stresses ahead of the tip varies markedly from that induced solely by the applied far-field loading.

2. Linear-elastic driving force calculations predict that cracks will follow a path where $K_{II} = 0$ (essentially equivalent to where G is maximum). Accordingly, for cracks at an interface where the far-field loading is mode I, cracks will kink away from the metal layer for bimaterial couples where the second Dundurs' parameter $\beta = 0$, irrespective of the value of the first Dundurs' parameter α; conversely, where $\alpha = 0$, cracks will kink into the metal layer for $\beta > 0$ and away from the layer if $\beta < 0$.

3. *For a crack lying in the interface,* the condition for it to leave the interface and kink into the matrix is governed by the relative toughness of the interface (G_{cIF}) and the matrix (G_c) for that phase angle, specifically by the relationship

$$\frac{G_{max}}{G_{IF}} > \frac{G_c}{G_{cIF}},$$

where G_{IF} is the driving force for interfacial crack extension, and G_{max} is the maximum driving force for extension into the matrix.

4. *For a crack impinging on an interface,* the condition governing whether the crack will deflect along the interface or penetrate it, is again given by the same expression. Specifically, for two linear elastic solids ($\alpha = \beta \sim 0$) under far-field tensile loads, the crack will deflect along the interface when $G_{cIF}/G_c < 1/4$. This condition is less stringent for bimaterial systems with a more positive α, and for cracks approaching the interface obliquely.

5. *For a crack near an interface,* linear-elastic projections imply that cracks will follow a straight parallel path if $K_{II} = 0$ and $\partial K_{II}/\partial c > 0$. For mode I far-field loading, however, three regimes of cracking configurations exist depending upon the value and sign of α and β.

6. Some, but not all, key trends for crack trajectory, and by implication for the pertinent fracture resistance, match the linear-elastic predictions for modulus mismatch effects; however, often the plastic zones in metal are too large relative to a layer thickness to confidently use computations based on elastic stress fields to deduce crack kinking tendencies.

7. At "weak" interfaces, the crack generally stays at the interface; near such interfaces, the crack will be drawn into the interface only if the compliance mismatch is such that β is positive. Where metal provides a "weak" path, cracks are drawn to the metal layer where $\beta > 0$, and deflected from the weak path where $\beta < 0$; here, the toughness G_c depends on the location and stability of a crack. However, where $\beta > 0$, the location of the crack path within the metal layer often does not match prediction, primarily because of plasticity within the layer. Where the ceramic provides the "weak" path, cracks deflect away from the metal layer and remain in the ceramic where $\beta < 0$. Where $\beta > 0$, conversely, cracks are drawn from the weak path to the "stronger" interface and metal; cracking configurations in this case can become complex, resulting in very high, but erratic, toughness values.

This work was supported by the Director, Office of Energy Research, Office of Basic Energy Sciences, Materials Sciences Division of the U.S. Department of Energy under Contract No. DE-AC03-76SF00098. Parts of this work were performed in collaboration with R. M. Cannon and J. M. McNaney.

REFERENCES

1. R. M. Cannon, B. J. Dalgleish, R. H. Dauskardt, J. M. McNaney, and R. O. Ritchie, *J. Am. Ceram. Soc.*, **78** (1995) (in review).
2. R. O. Ritchie, R. M. Cannon, B. J. Dalgleish, R. H. Dauskardt, and J. M. McNaney, *Mater. Sci. Eng.*, **A166**, 221 (1993).
3. F. Erdogan and G. C. Sih, *J. Basic Eng.*, **85**, 519 (1963).
4. B. Cotterell, *Int. J. Fract. Mech.*, **1**, 96 (1965).
5. B. A. Bilby and G. E. Cardew, *Int. J. Fract.*, **11**, 708 (1975).
6. B. A. Bilby, G. E. Cardew, I. C. Howard, and D. M. R. Taplin, *Fracture 1977, Advances in Research on the Strength and Fracture of Materials*, Vol. 3, Pergamon Press, Oxford (1977), p. 197.
7. B. Cotterell and J. W. Rice, *Int. J. Fract.*, **16**, 155 (1980).
8. K. K. Lo, *J. Appl. Mech.*, **45**, 797 (1978).

9. K. Palaniswamy and W. G. Knauss, in: S. Nemat-Nasser (editor), *Mechanics Today*, Vol. 4, Pergamon Press, Oxford (1978), p. 87.
10. S. Nemat-Nasser and H. Hori, *J. Geophys. Research*, **87**, 6805 (1982).
11. M.-Y. He and J. W. Hutchinson, *J. Appl. Mech.*, **56**, 270 (1989).
12. B. Cotterell, *Int. J. Fract. Mech.*, **2**, 526 (1966).
13. J. W. Hutchinson and Z. Suo, *Adv. Appl. Mech.*, **29**, 63 (1991).
14. J. G. Williams and P. D. Ewing, *Int. J. Fract. Mech.*, **8**, 441 (1972).
15. I. Finnie and A. Saith, *Int. J. Fract.*, **9**, 484 (1973).
16. P. D. Ewing, J. L. Swedlow, and J. G. Williams, *Int. J. Fract.*, **12**, 85 (1976).
17. J. R. Rice, *J. Appl. Mech.*, **55**, 98 (1988).
18 J. W. Hutchinson, M. E. Mear, and J. R. Rice, *J. Appl. Mech.*, **54**, 828 (1987).
19. C. F. Shih and R. J. Asaro, *J. Appl. Mech.*, **55**, 299 (1988).
20. J. J. Dundurs, *J. Appl. Mech.*, **36**, 650 (1969).
21. Z. Suo and J. W. Hutchinson, *Mater. Sci. Eng.*, **A107**, 135 (1989).
22. C. F. Shih and R. J. Asaro, *J. Appl. Mech.*, **55**, 299 (1988).
23. C. F. Shih, R. J. Asaro, and N. P. O'Dowd, *J. Appl. Mech.*, **58**, 450 (1991).
24. Z. Suo and C. F. Shih, in: S. Suresh, A. Mortensen, and A. Needleman (editors), *Fundamentals of Metal-Matrix Composites*, Butterworths (1993), p. 217.
25. C. Woeltjen, C. F. Shih, and S. Suresh, *Acta Metall. Mater.*, **41**, 2317 (1993).
26. M.-Y. He, A. Bartlett, A. G. Evans, and J. W. Hutchinson, *J. Am. Ceram. Soc.*, **74**, 767 (1991).
27. M.-Y. He and J. W. Hutchinson, *Int. J. Solids Struct.*, **25**, 1053 (1989).
28. A. G. Evans, M.-Y. He, and J. W. Hutchinson, *J. Am. Ceram. Soc.*, **72**, 2300 (1989).
29. N. A. Fleck, J. W. Hutchinson, and Z. Suo, *Int. J. Solids Struct.*, **27**, 1683 (1991).
30. J. M. McNavey, R. M. Cannon, and R. O. Ritchie, *Int. J. Fract.*, **66**, 227 (1994).